THE JOURNAL OF PHYSICAL CHEMISTRY C

pubs.acs.org/JPCC Article

High-Speed Direct Writing of $MoSe_2$ by Maskless and Gas-Free Laser-Assisted Selenization Process

Yoonsoo Rho,[$] Healin Im,[$] Letian Wang, Matthew Eliceiri, Brian Blankenship, Sunkook Kim,* and Costas P. Grigoropoulos*

Cite This: *J. Phys. Chem. C* 2020, 124, 19333−19339 Read Online

ACCESS | Metrics & More | Article Recommendations | Supporting Information

ABSTRACT: Transition metal dichalcogenides (TMDCs) have shown exceptional optoelectronic properties that can potentially substitute conventional silicon-based devices and be utilized in sensors and energy devices. To exploit their wide array of potential applications, it is necessary to develop methods capable of on demand, location selective, and tunable formation of structures of arbitrary shape. Here, we demonstrated high-speed direct writing of $MoSe_2$ by laser-induced selenization process in vacuum or ambient environment. Laser irradiation on predeposited Se/Mo multilayer promptly forms polycrystalline $MoSe_2$ in a site-selective manner without use of photomask and toxic gas. *In situ* reflectance measurement and temperature simulation identified distinct characteristic processing stages, revealing that the time required for synthesizing ∼20 nm-thick $MoSe_2$ polycrystal film is of the order of 10^{-3}s, which is significantly faster than the conventional selenization process using furnace annealing. We believe that the laser synthesis of $MoSe_2$ demonstrated in this study is of general applicability and therefore offers a simple and straightforward route for obtaining arbitrary patterns in TMDCs.

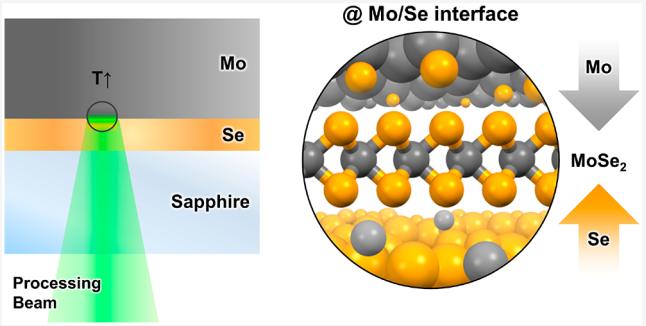

INTRODUCTION

TMDCs have attracted significant interest due to their outstanding optoelectronic properties, such as relatively large band gap (1.2−1.9 eV) with moderate mobility at room temperature (up to ∼200 $cm^2/V{\cdot}s$),[1−3] as well as rich exciton dynamics when reduced to mono- or few-layers.[4] In addition, their mechanical flexibility and highly tunable properties are advantageous for high-performance flexible electronics.[5,6] Such promising properties are attributed to the multiple van der Waals stacked atomically thin layers that are terminated by covalently bonded atoms and relatively free of surface defects. In turn, TMDCs are often recalled as alternatives to silicon-based nanoscale electronics that suffer from intrinsic surface defects that significantly impair charge transport performances.[7]

Although TMDCs are highly promising, technological developments in defining their shape and location still experience bottlenecks that hinder efforts to substitute conventional bulk materials. As a bottom-up approach, it has been shown that chemical vapor deposition (CVD) can form mono- or few- layer TMDCs in large area, followed by shape definition using a mask-based CMOS process.[8,9] However, this approach generated random seeding, as the initial nucleation site affected the continuity and imposed time-consuming lateral growth processes. In this regard, sulfurization or selenization of predefined metal films (i.e., molybdenum (Mo) or Tungsten (W)) may offer a rather straightforward route to form TMDCs by controlling solely chalcogen gas (i.e., Sulfur (S) or Selenium (Se)).[10−17] On the basis of this method, synthesis of mono- or few- layer MoS_2,[11,13−15] WS_2,[12,15,16] and WSe_2[17] have been demonstrated. However, those methods require prolonged heating and cooling time under toxic gas flow, which is not applicable to sensitive and flexible substrates. Furthermore, it requires photolithography steps to define the shape and location of the TMDCs.

Laser has been considered as the most feasible means to supply local energy for materials modification by providing photons in temporally and spatially controlled manner.[18,19] Thus, without using wet photolithography processes, arbitrary shapes can be readily produced rapidly and site-selectively. In this regard, laser has been implemented as a clean and precise processing tool for the local thinning,[20,21] patterning, and doping[22] of TMDCs. Despite its advantages, synthesis of TMDCs by laser has not been introduced yet, which is partly ascribed to the difficulty in controlling sensitive stoichiometry

Received: May 31, 2020
Revised: August 8, 2020
Published: August 10, 2020

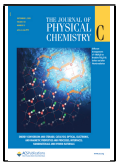

https://dx.doi.org/10.1021/acs.jpcc.0c04914
J. Phys. Chem. C 2020, 124, 19333−19339

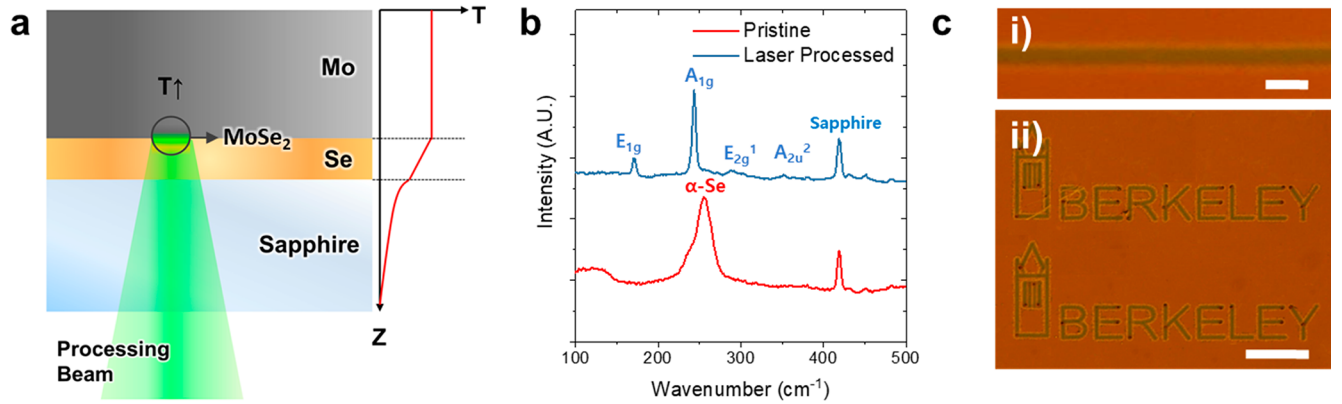

Figure 1. (a) Schematic of the laser-induced $MoSe_2$ synthesis in sapphire/Se/Mo multilayer. The laser beam was irradiated through the transparent sapphire substrate, and $MoSe_2$ was formed at Se/Mo interface. The temperature profile shows linear drops in the Se layer, exponential drops in sapphire, and almost no change in the Mo layer. (b) Raman spectra obtained from the pristine and laser-processed area. (c) Optical microscope images obtained through the sapphire substrate show (i) simple line and (ii) arbitrary patterns. The scale bars in panels (i) and (ii) indicate 10 and 100 μm, respectively.

in case of CVD growth by the locally varying laser-induced temperature.

Here, we demonstrate direct writing of $MoSe_2$ based on Mo and Se multilayers by laser-induced selenization process. Raman, X-ray photoelectron spectroscopy (XPS), and transmission electron microscopy (TEM) analyses confirmed the formation of polycrystalline $MoSe_2$ at the interface between Mo and Se layers. We interrogated the laser processing parameters for $MoSe_2$ synthesis and identified distinct characteristic synthesis stages by applying *in situ* reflectance measurement and temperature simulation. The time required for the formation of a 20 nm-thick layer of $MoSe_2$ was found to be of the order of 10^{-3}s, which is much shorter than that of CVD and sulfurization or selenization by furnace annealing. Thus, our new approach allows fast formation of arbitrary TMDC patterns in microscale resolutions for various future potential applications.

METHODS

Preparation of Se-Mo Films on Sapphire Substrate. A Se layer (25 nm) was deposited on a sapphire substrate using RF sputtering under 100 sccm of Ar flow, and the RF power was set as 15 W. The pressure was 10 mTorr during the deposition, whereas the base pressure was 4.0×10^{-6} Torr. During the deposition of the Mo layer (100 nm), the RF power was 150 W under the same Ar flow rate. The pressure during the deposition was 10 mTorr.

Laser-Induced Selenization Process. A CW 532 nm laser (Sprout, 5W) was focused through a 10X objective lens (NA ~ 0.28). The sample was placed in a stainless-steel chamber equipped with a quartz window for optical access. A dichroic mirror placed between the objective lens and zoom lens allowed optical monitoring during the processing. For vacuum processing, the pressure was maintained below 1 mTorr. For preparation of the sample for the Raman, XPS, and TEM analyses and *ex-situ* reflectance measurement, the laser-induced selenization process was conducted under a vacuum, while we conducted the *in situ* reflectance measurement at ambient environment conditions.

Characterization. A CW 532 nm laser focused by a 50X objective lens and 1800 cm^{-1} grating was used for Raman measruement (inVia, Renishaw), and the power was maintained below 0.5 mW to avoid any damage to the sample. XPS depth profiling was performed using an XPS spectrometer (K-Alpha+, ThermoFisher Scientific. Co.). The XPS spectra were calibrated at the C 1s peak of 285.0 eV. Cross-sectional TEM and STEM images were obtained using analytic STEM (JEM-2100F, JEOL Co.).

***In Situ* reflectance measurement.** *In situ* reflectance measurement was performed at ambient condition. A He−Ne laser (wavelength: 633 nm) was coupled as a probing beam. A polarized beam splitter (PBS) coaxially combines the probing beam to the processing beam (532 nm) before the objective lens. A beam expander was used to expand the probing beam to adjust the focal spot size of the 633 nm beam to be smaller than the focal spot of the processing beam. A quarter wave plate located between the PBS and the objective lens performs half-wave retardation when the probing beam passes through it twice, allowing it to pass through the PBS directed to the avalanche photo diode (APD) after color filters that block the probing beam. The processing beam was modulated using an acoustic optical modulator (AOM) such that the rise and decay times of laser beam irradiation are controlled within 2 μs. The beam splitter split a fraction of the processing beam directly to a photodiode to trigger an oscilloscope that recorded the *in situ* change in the 633 nm power registered at the APD. The schematic diagram is included in the Supporting Information.

Heat Transfer Simulation. The details are described in the Supporting Information.

RESULTS AND DISCUSSION

Amorphous Se (a-Se) (25 nm) and Mo (100 nm) layers were deposited on a sapphire substrate by radio frequency (RF) sputtering. The thicknesses of deposited a-Se and Mo layers were determined by AFM and SEM cross-sectional analysis. An as-prepared Se/Mo multilayer sample was placed in a processing chamber equipped with quartz window allowing laser-assisted synthesis of $MoSe_2$ under vacuum or ambient conditions. A continuous wave (CW) laser beam (λ = 532 nm) was irradiated through the transparent sapphire substrate (Figure 1a) and focused via an objective lens (numerical aperture (NA) ~ 0.28) resulting in a spot size of ~5.4 μm ($1/e^2$) at Se/Mo interface. This processing scheme allowed the *in situ* monitoring of $MoSe_2$ synthesis, whereas the opaque Mo layer prevented optical inspection. The laser fluence impinging

https://dx.doi.org/10.1021/acs.jpcc.0c04914
J. Phys. Chem. C 2020, 124, 19333−19339

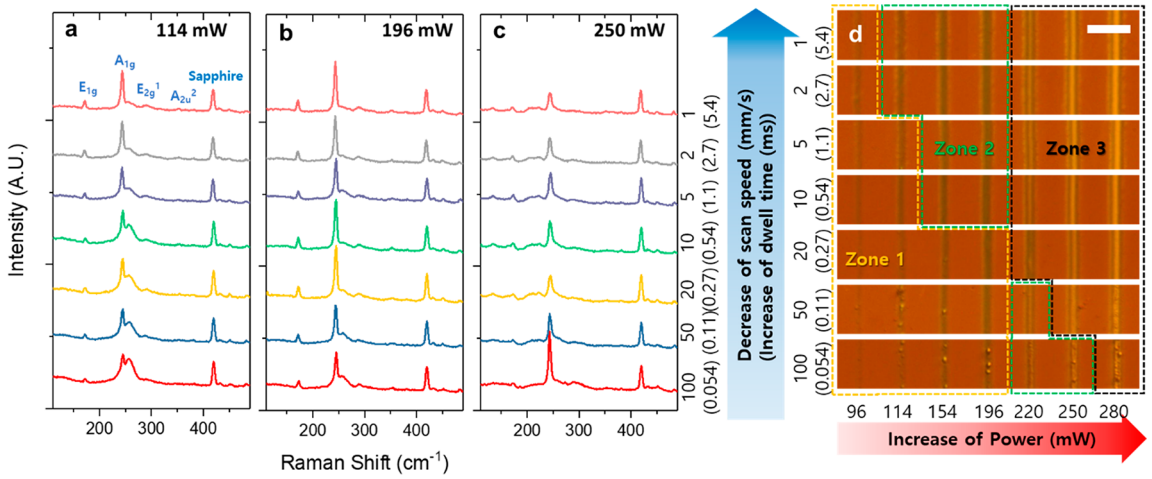

Figure 2. Raman spectra and optical microscope images obtained by varying laser power and scan speed at vacuum condition show distinct characteristic processing stages. Raman spectra at a fixed laser power of (a) 114 mW, (b) 196 mW, and (c) 250 mW for varying laser scan speeds (mm/s) (dwell time (ms)). (d) Laser fluence (mW) with respect to scan speed (mm/s) (dwell time (ms)) diagram consisting of optical microscope images of synthesized $MoSe_2$ lines. The dashed boxes explicitly show the distinct processing regions, zone 1 (yellow), zone 2 (green), and zone 3 (black). The scale bar indicates 20 μm.

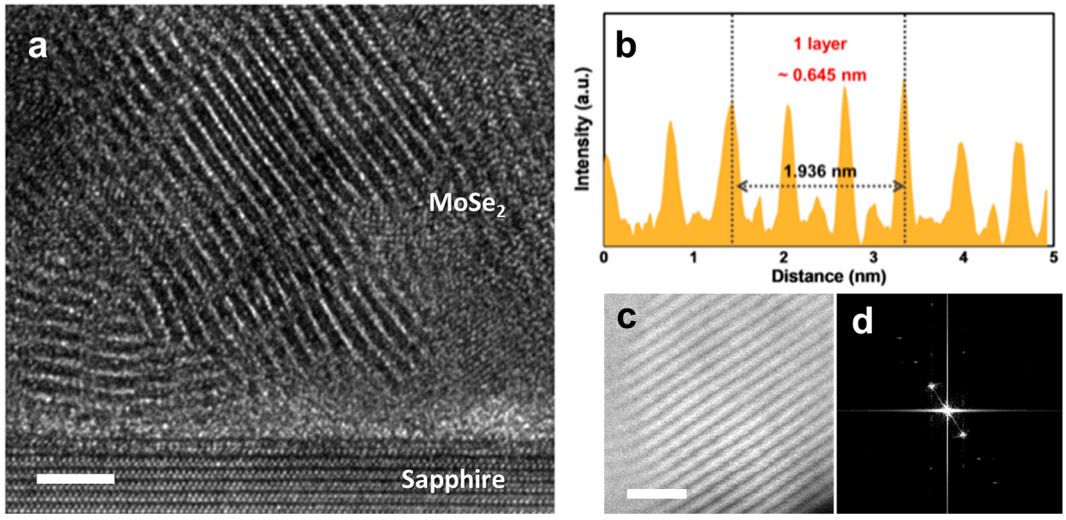

Figure 3. (a) Cross-sectional TEM image taken from the interface between sapphire and $MoSe_2$ after laser processing using a laser fluence of 196 mW at a scan speed (dwell time) of 2 mm/s (2.7 ms), corresponding to zone 2. (b) Line profiles of interlayer spacing show 6.45 Å between layers. (c) STEM and (d) FFT images obtained from the $MoSe_2$ region. The scale bars indicate 3 nm.

on the sample was mostly absorbed by the Mo-layer due to its large extinction coefficient (k ~ 7.18), while Se and sapphire exhibit orders of magnitude smaller values (k ~ 0.106 and k ~ 0, respectively). Despite its thinness, the Se layer possesses a low thermal conductance of 21 $MW/m^2 \cdot K$ ($\sim k/L$, where k and L indicate thermal conductivity (0.519 W/m·K) and thickness (25 nm) of Se layer, respectively). The inefficient heat conduction through the Se layer induced a sharp drop in temperature. Further, we note that the Se layer was sandwiched between the substrate and the Mo layer to mitigate the evaporation of Se during laser processing. In contrast, the Se layer deposited on top of the Mo layer easily evaporated at relatively low laser fluence owing to its low melting and boiling temperatures (494 and 958 K, respectively). After processing using a laser fluence of 196 mW at 2 mm/s of scan speed, the Raman spectra clearly changed as shown in Figure 1b. Raman spectra from pristine $MoSe_2$ sample showed a broad a-Se peak at 260 cm^{-1} while sharp peaks at 170 cm^{-1}, 242 cm^{-1}, 288 cm^{-1}, and 352 cm^{-1} indicated formation of 2H-$MoSe_2$, which corresponded to phonon vibration modes at E_{1g}, A_{1g}, $E_{2g}{}^1$, and $A_{2u}{}^2$, respectively. Note that all the optical measurements, including Raman spectra and optical microscopy, were collected through the transparent sapphire substrate. Distinct color changes indicating the formation of $MoSe_2$ were observed in the optical microscope images. The interference in multithinlayer film structure sensitively changed the reflectance spectra depending on the material thickness. Such a site-selective synthesis scheme allowed the formation of $MoSe_2$ patterns of arbitrary shape (Figure 1c-ii).

Raman spectra were obtained by varying both laser power and scan speed and are shown in Figure 2a–c. Note that the scan speed is connected to the dwell time of the laser beam (v/w, where v and w are the laser spot size and scan speed, respectively). At a laser fluence of 114 mW (Figure 2a), which is close to the threshold of initiating the synthesis of $MoSe_2$,

https://dx.doi.org/10.1021/acs.jpcc.0c04914
J. Phys. Chem. C 2020, 124, 19333−19339

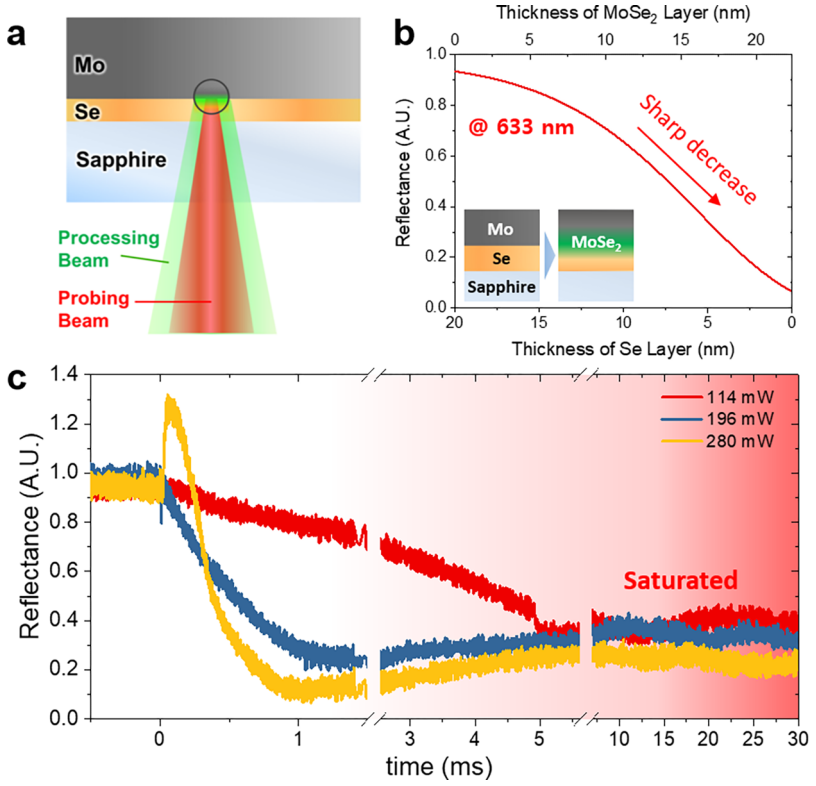

Figure 4. *In situ* reflectance measurement showing the processing time for the saturation of $MoSe_2$ synthesis. (a) Schematic illustration of the *in situ* reflectance measurement utilizing coaxially coupled probing and processing beams. (b) Calculated reflectance of the Se/$MoSe_2$/Mo multilayer at a wavelength of 633 nm incident from the sapphire side as a function of the thicknesses of the Se layer and the $MoSe_2$ layer formed. (c) Measured *in situ* reflectance data depending on the incident processing laser power. The plots correspond to incident laser powers of 114, 196, and 280 mW, indicated by the red, blue, and yellow lines, respectively.

A_{1g} and E_{1g} peaks start to appear at a scan speed (dwell time) of 100 mm/s (0.054 ms), while a-Se peak near 260 cm^{-1} remained prominent. Upon lowering the scan speed (leading to an increased dwell time), the intensity of a-Se peak gradually diminished and was dominated by $MoSe_2$ peaks to finally disappear at 1 mm/s (5.4 ms). This result indicates that the time required for saturation of the interdiffusion of Mo and Se layers to form $MoSe_2$ was ~5 ms at this processing parameter. Figure 2d compiles the optical microscope images depicting the laser fluence versus scan speed dependence. In this figure, we have marked the characteristic processing regions by dashed lines. Zone 1 indicates the mixture of a-Se and $MoSe_2$, whereas zone 2 shows saturation of $MoSe_2$ formation. The gradual color change in the optical microscope images is a manifestation of the decrease in the thickness of Se-layer, accompanying the formation of the $MoSe_2$ layer. As we increased the laser fluence to 196 mW, the transition from zone 1 to zone 2 occurred faster at ~0.5 ms (Figure 2b). At higher laser fluence (230 mW), the a-Se peak immediately disappeared at 100 mm/s (0.054 ms) and the intensity of the $MoSe_2$ peaks decreased abruptly (Figure 2c). The optical microscope images in zone 3 showed scan lines of bright metallic color, which are ascribed to the Mo surface being exposed by the fast interdiffusion of Mo and Se without the formation of high-quality $MoSe_2$.

The TEM images show that polycrystalline 2H-$MoSe_2$ was formed at the interface between Mo and Se layers, as shown in Figure 3. The TEM sample was prepared using a scan speed (dwell time) 2 mm/s (5.4 ms) that induced saturation of the process (zone 2) at 196 mW. We occasionally observed voids formed between the sapphire substrate and $MoSe_2$ (Figure S1). We attribute this void formation to the volume shrinkage (12.7%) upon formation of $MoSe_2$ in case of ideal stoichiometry (i.e., molar ratio; Mo/Se = 1:2) and/or organic contamination introduced during the sample preparation. Nevertheless, a clear 2H phase $MoSe_2$ structure was observed from the zone 2 sample (Figure 3a) with an interlayer distance (along *c*-axis) of 0.645 Å. These findings were confirmed by TEM image and fast Fourier transform (FFT) pattern (Figure 3b,c). The diffraction pattern from a discrete and ordered dot shows the crystalline orientation along the *c*-axis (Figure 3d). In addition, the grain size was ~20 nm (Figure S1), which is in a range similar to the previously reported MoS_2, WS_2, or WSe_2 synthesized via gas phase sulfurization or selenization of transition metal films.[10−14] Meanwhile, the results obtained from the laser-processed region corresponding to zone 1 (using a laser fluence of 114 mW at a scan speed of 2 mm/s) show smaller grain sizes mixed with a-Se (Figure S2), which can be directly correlated with the Raman spectra of zone 1. In addition, the clear shifts in elemental bonding status can be observed using XPS depth profiling obtained from zone 2 sample (Figure S3). As we collected XPS spectra from the top Mo layer to the sapphire substrate, the Mo $3d_{5/2}$ and Mo $3d_{3/2}$ peaks abruptly blue-shifted at the interface between Mo and $MoSe_2$ layers, whereas the Se 3d peak appeared simultaneously. The blue shift in Mo 3d peaks implies the increased oxidation number of the elements, indicating the formation of Mo−Se bonding.[23] The peak widths were broadened compared to those of pristine 2H-$MoSe_2$, which were affected

https://dx.doi.org/10.1021/acs.jpcc.0c04914
J. Phys. Chem. C 2020, 124, 19333−19339

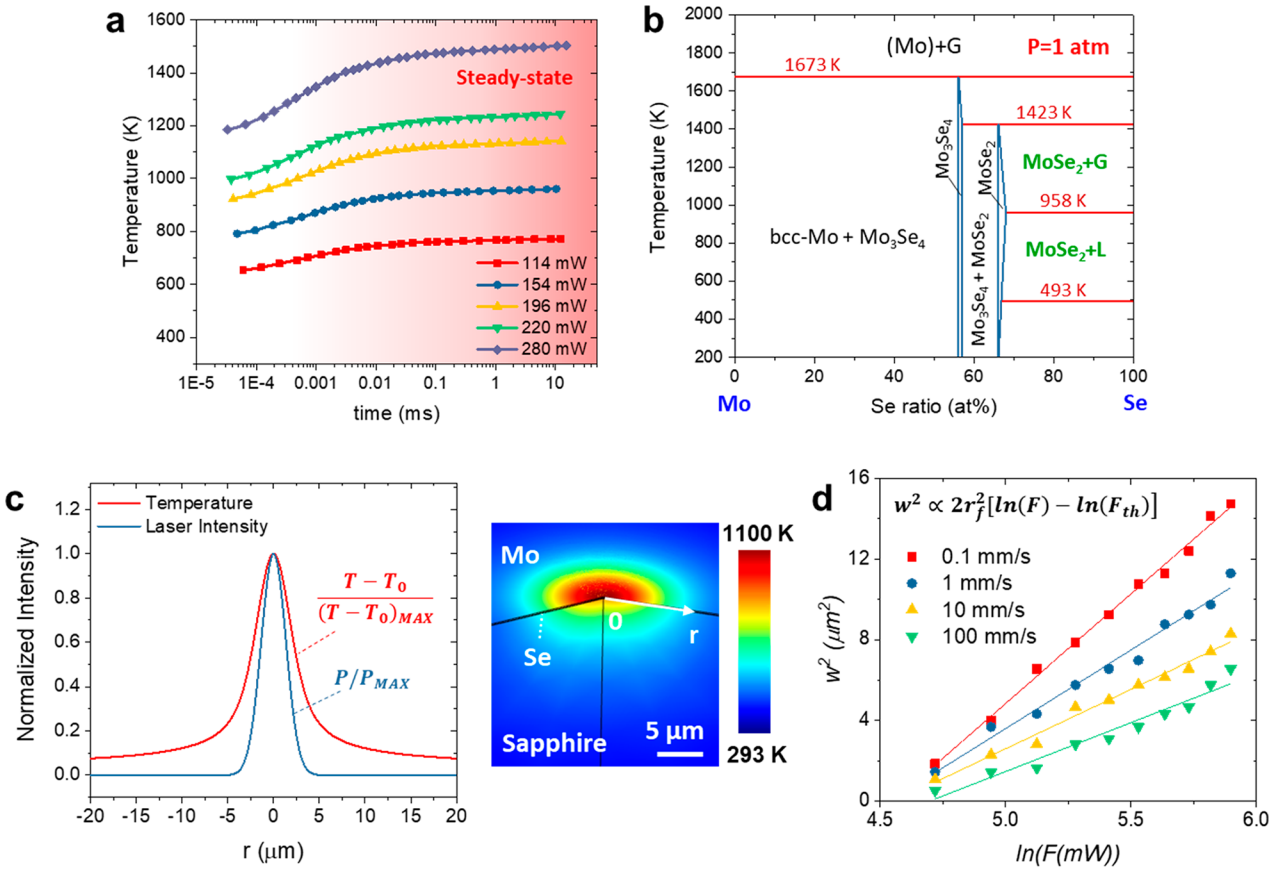

Figure 5. (a) Simulated peak temperatures at the interface between Mo and Se layers for incident laser powers of 112, 154, 196, 220, and 280 mW. (b) Mo−Se temperature composition (T-x) phase diagram at a pressure of 1 atm.[27] (c) Normalized temperature and laser power profiles along the r direction, as indicated in the right panel. Right panel: Simulated temperature field of the Se/Mo multilayer at a laser fluence of 196 mW after 10 ms. (d) Square of width of the $MoSe_2$ pattern (w^2) versus the logarithmic value of the laser fluence ($ln(F)$) obtained from various scan speeds.

by presence of defects and multi grain boundaries of polycrystalline structure.[24,25]

The processing time required for $MoSe_2$ synthesis was experimentally probed by *in situ* reflectance measurements at ambient environment conditions. A He−Ne laser beam ($\lambda \sim$ 633 nm) coaxially aligned with the processing laser ($\lambda \sim$ 532 nm) allowed the real-time probing of the change in reflectance at 633 nm (Figure 4a). Using thin film optics,[26] the reflectance of multilayer structure (sapphire/Se/$MoSe_2$/Mo) at 633 nm can be deduced, depending on the Se thickness and corresponding synthesized $MoSe_2$ layer as shown in Figure 4b (the details of the derivation are provided in Supporting Information). The reflectance decreased sharply as Se was consumed into $MoSe_2$, and the ratio of changes in thicknesses of Se and $MoSe_2$ was calculated as 1.12 (Supporting Information). The *in situ* measured reflectance data at various laser fluences are depicted in Figure 4c. At a low laser fluence (114 mW), the reflectance gradually decreased until ∼6 ms and saturated. At moderate laser fluence (196 mW), it decreased faster during the earlier stage and until ∼1 ms. At high fluence (280 mW), the reflectance rose sharply and dropped suddenly. The fast interlayer diffusion exposed the Mo surface without the formation of $MoSe_2$, thereby increasing the reflectance during the early stage. The subsequent fast oxidation of Mo layer starting from the top surface produced volatile MoOx, that could be easily released. This process resulted in a sharp drop in the reflectance. The experimental *ex situ* reflectance measurement from the sample prepared at vacuum condition (Figure S4) showed a similar trend, except for the high laser fluence (280 mW) that was marked by increased and sustained reflectance due to the absence of oxidation of Mo film. On the basis of this result, we deduced that the time scale required for $MoSe_2$ synthesis was in the range of 1−6 ms, depending on the laser fluence, which was significantly faster than the conventional selenization or sulfurization process using the furnace annealing method (∼hours).[10−14]

The high-speed and spatially confined processing was primarily enabled by the rapid temperature change induced by focused laser power. We modeled the temporal and spatial temperature distribution using finite element method (FEM) based on the sapphire/Se/Mo multilayer structure as shown in Figure 5 (details are provided in the Supporting Information). Figure 5a shows the transient temperature at the center of the irradiated spot during laser heating of a nonmoving sample. The temperature profile developed rapidly within 10^{-2} ms, which is much shorter than the time for the saturation of processing (1−6 ms). At the threshold fluence (∼114 mW) that corresponds to the zone 1, the temperature increased up to ∼600 K, while at highest fluence (280 mW) (zone 3), it reached up to 1500 K. Figure 5b shows a Mo-Se-temperature-composition (T-x) phase diagram at a pressure of 1 atm.[27] The $MoSe_2$ synthesis is expected to occur within the temperature range of 493−1423 K, where a mixture of $MoSe_2$ and Se in either gaseous or liquid phase is present atomic ratio of Se exceeding 0.66. In addition to the fast temporal temperature

https://dx.doi.org/10.1021/acs.jpcc.0c04914
J. Phys. Chem. C 2020, 124, 19333−19339

profile, the lateral profile shows favorable microscale confinement (Figure 5c). We note that the simulation was based on laser power of 196 mW and dwell time of 10 ms. The full width half-maximum (fwhm) of normalized temperature profile ($\frac{T-T_0}{(T-T_0)_{max}}$ where T_0 is the room temperature) along the r direction in Figure 5a was estimated to be 5.3 μm, which is slightly larger than the fwhm of laser beam intensity profile of 3.4 μm ($\sim\sqrt{\ln 2/2}\cdot w$ where w is $1/e^2$ width, 5.7 μm). The pattern widths shown in Figure 2d are in a range similar to the fwhm of the temperature profile. Also, for Gaussian-like temperature profile, the width of the processed area (w) is related to the laser fluence (F) by $w^2 \propto 2r_f^2[ln(F) - ln(F_{th})]$, where r_f and F_{th} are the radii of $1/e^2$ laser focal spot (5.4 μm) and threshold fluence that can initiate the process, respectively. The equation can correlate the measured pattern width with the laser fluence as shown in Figure 5d. In addition, the intercept of the extrapolated line at $w = 0$ should indicate the F_{th}. As anticipated, this procedure yields identical value of ~95 mW for various scan speeds.

Despite the fast processing scheme of the order of 10^{-3}s, the kinetics of the laser-assisted selenization can be quantified by the mass diffusion equation using the estimated temperature and measured processing time. The corresponding formula and constants were introduced by Shin et al.[28] based on the selenization of thick Mo film (~3 μm) by furnace annealing under Se vapor atmosphere. The $MoSe_2$ thickness (L_{MoSe_2}) can be formulated by $L_{MoSe_2} = \sqrt{2\frac{C_{Se,0}}{C_{Se,1}}D_{MoSe_2}t}$ where $C_{Se,0}$ and $C_{Se,1}$ are Se atomic densities in fully covered Se layer on Mo surface (3.7×10^{22} cm^{-3}) and in $MoSe_2$ crystal (1.1×10^{22} cm^{-3}), respectively. D_{MoSe_2}, which is the diffusion coefficient of Se in $MoSe_2$, is given by $D_{MoSe_2} = D_{MoSe_2,0}\exp\left(-\frac{E_{D_{MoSe_2}}}{KT}\right)$ where $D_{MoSe_2,0}$ and $E_{D_{MoSe_2}}$ are a prefactor (5.5×10^{-7} cm^2/s) and the activation energy of $MoSe_2$ formation (0.68 eV), respectively. In our sample configuration, Se was provided by solid Se layer, which can satisfy the assumption of fully covered Se layer on Mo and $MoSe_2$ surface. With the substitution of 900 K and 2.7 ms (corresponding to the saturation of processing at zone 2), L_{MoSe_2} was estimated as 12.5 nm, which is similar to the synthesized $MoSe_2$ as shown in the TEM image. As the diffusion of Se occurs mainly through grain boundaries of $MoSe_2$, the nonuniformity of the polycrystals in our case can affect the local D_{MoSe_2}, resulting in uneven thickness of the produced $MoSe_2$. Thus, the results indicate that the high-speed laser processing induced $MoSe_2$ formation, in our study, is consistent with the diffusion kinetics based on bulk films.

CONCLUSIONS

We demonstrated high-speed direct writing $MoSe_2$ by laser-assisted selenization. Arbitrary patterns of $MoSe_2$ could be written from a Se/Mo multilayer at vacuum or ambient conditions. Raman, XPS, and TEM analyses revealed the formation of polycrystalline 2H-$MoSe_2$ at the interface between Mo and Se. On the basis of the *in situ* reflectance measurement and the temperature simulation, we revealed that the high-speed processing was enabled by the rapid temperature increase induced by laser. The diffusion model is shown to be well suited for the interpretation of our results. We believe that our investigation provides useful insight into the utilization of laser-assisted selenization or sulfurization processes for the location selective synthesis and arbitrary shape patterning of TMDC materials.

ASSOCIATED CONTENT

Supporting Information

The Supporting Information is available free of charge at https://pubs.acs.org/doi/10.1021/acs.jpcc.0c04914.

Cross-sectional TEM images taken from zone 1 and zone 2; XPS depth profiles of Mo 3d and Se 3d core peaks from zone 2; ex-situ reflectance data; optical microscope images and Raman spectra of $MoSe_2$ obtained at ambient condition; methods to calculate the reflectance of multilayer thin films; methods to calculate the volume change of films as a result of laser-induced selenization process; details of heat transfer simulation; schematics of *in situ* reflectance measurement set up (PDF)

AUTHOR INFORMATION

Corresponding Authors

Costas P. Grigoropoulos − *Laser Thermal Laboratory, Department of Mechanical Engineering, University of California, Berkeley, California 94720, United States;* orcid.org/0000-0002-8505-4037; Email: cgrigoro@berkeley.edu

Sunkook Kim − *School of Advanced Materials Science and Engineering, Sungkyunkwan University, Suwon-si, Gyeonggi-do 16419, Republic of Korea;* orcid.org/0000-0003-1747-4539; Email: seonkuk@skku.edu

Authors

Yoonsoo Rho − *Laser Thermal Laboratory, Department of Mechanical Engineering, University of California, Berkeley, California 94720, United States*

Healin Im − *School of Advanced Materials Science and Engineering, Sungkyunkwan University, Suwon-si, Gyeonggi-do 16419, Republic of Korea*

Letian Wang − *Laser Thermal Laboratory, Department of Mechanical Engineering, University of California, Berkeley, California 94720, United States*

Matthew Eliceiri − *Laser Thermal Laboratory, Department of Mechanical Engineering, University of California, Berkeley, California 94720, United States*

Brian Blankenship − *Laser Thermal Laboratory, Department of Mechanical Engineering, University of California, Berkeley, California 94720, United States*

Complete contact information is available at: https://pubs.acs.org/10.1021/acs.jpcc.0c04914

Author Contributions

$Both authors contributed equally.

Notes

The authors declare no competing financial interest.

ACKNOWLEDGMENTS

Financial support awarded to the University of California, Berkeley, by the U.S. National Science Foundation (Grant No. CMMI-1662475) is gratefully acknowledged. This research was also supported by the National Research Foundation of Korea (Grant No. NRF-2018R1A2B2003558).

REFERENCES

(1) Xia, F.; Wang, H.; Xiao, D.; Dubey, M.; Ramasubramaniam, A. Two-Dimensional Material Nanophotonics. *Nat. Photonics* **2014**, *8*, 899−907.

(2) Cui, X.; Lee, G.-H.; Kim, Y. D.; Arefe, G.; Huang, P. Y.; Lee, C.-H.; Chenet, D. A.; Zhang, X.; Wang, L.; Ye, F.; et al. Multi-Terminal Transport Measurements of Mos2 Using a Van Der Waals Heterostructure Device Platform. *Nat. Nanotechnol.* **2015**, *10*, 534−540.

(3) Kim, S.; Konar, A.; Hwang, W.-S.; Lee, J. H.; Lee, J.; Yang, J.; Jung, C.; Kim, H.; Yoo, J.-B.; Choi, J.-Y. High-Mobility and Low-Power Thin-Film Transistors Based on Multilayer MoS2 Crystals. *Nat. Commun.* **2012**, *3*, 1−7.

(4) Mak, K. F.; Lee, C.; Hone, J.; Shan, J.; Heinz, T. F. Atomically Thin ${\Mathrm{Mos}}_{2}$: A New Direct-Gap Semiconductor. *Phys. Rev. Lett.* **2010**, *105*, 136805.

(5) Akinwande, D.; Brennan, C. J.; Bunch, J. S.; Egberts, P.; Felts, J. R.; Gao, H.; Huang, R.; Kim, J.-S.; Li, T.; Li, Y.; et al. A Review on Mechanics and Mechanical Properties of 2d Materials—Graphene and Beyond. *Extreme Mechanics Letters* **2017**, *13*, 42−77.

(6) Kwon, H.; Choi, W.; Lee, D.; Lee, Y.; Kwon, J.; Yoo, B.; Grigoropoulos, C. P.; Kim, S. Selective and Localized Laser Annealing Effect for High-Performance Flexible Multilayer Mos 2 Thin-Film Transistors. *Nano Res.* **2014**, *7*, 1137−1145.

(7) Jin, S.; Fischetti, M. V.; Tang, T.-W. Modeling of Surface-Roughness Scattering in Ultrathin-Body Soi Mosfets. *IEEE Trans. Electron Devices* **2007**, *54*, 2191−2203.

(8) Wang, X.; Gong, Y.; Shi, G.; Chow, W. L.; Keyshar, K.; Ye, G.; Vajtai, R.; Lou, J.; Liu, Z.; Ringe, E. Chemical Vapor Deposition Growth of Crystalline Monolayer Mose2. *ACS Nano* **2014**, *8*, 5125−5131.

(9) Jung, C.; Kim, S. M.; Moon, H.; Han, G.; Kwon, J.; Hong, Y. K.; Omkaram, I.; Yoon, Y.; Kim, S.; Park, J. Highly Crystalline Cvd-Grown Multilayer Mose 2 Thin Film Transistor for Fast Photo-detector. *Sci. Rep.* **2015**, *5*, 1−9.

(10) Chiappe, D.; Asselberghs, I.; Sutar, S.; Iacovo, S.; Afanas'ev, V.; Stesmans, A.; Balaji, Y.; Peters, L.; Heyne, M.; Mannarino, M. Controlled Sulfurization Process for the Synthesis of Large Area Mos2 Films and Mos2/Ws2 Heterostructures. *Adv. Mater. Interfaces* **2016**, *3*, 1500635.

(11) Lee, Y.; Lee, J.; Bark, H.; Oh, I.-K.; Ryu, G. H.; Lee, Z.; Kim, H.; Cho, J. H.; Ahn, J.-H.; Lee, C. Synthesis of Wafer-Scale Uniform Molybdenum Disulfide Films with Control over the Layer Number Using a Gas Phase Sulfur Precursor. *Nanoscale* **2014**, *6*, 2821−2826.

(12) Song, J.-G.; Park, J.; Lee, W.; Choi, T.; Jung, H.; Lee, C. W.; Hwang, S.-H.; Myoung, J. M.; Jung, J.-H.; Kim, S.-H. Layer-Controlled, Wafer-Scale, and Conformal Synthesis of Tungsten Disulfide Nanosheets Using Atomic Layer Deposition. *ACS Nano* **2013**, *7*, 11333−11340.

(13) Tarasov, A.; Campbell, P. M.; Tsai, M. Y.; Hesabi, Z. R.; Feirer, J.; Graham, S.; Ready, W. J.; Vogel, E. M. Highly Uniform Trilayer Molybdenum Disulfide for Wafer-Scale Device Fabrication. *Adv. Funct. Mater.* **2014**, *24*, 6389−6400.

(14) Zhan, Y.; Liu, Z.; Najmaei, S.; Ajayan, P. M.; Lou, J. Large-Area Vapor-Phase Growth and Characterization of Mos2 Atomic Layers on a Sio2 Substrate. *Small* **2012**, *8*, 966−971.

(15) Orofeo, C. M.; Suzuki, S.; Sekine, Y.; Hibino, H. Scalable Synthesis of Layer-Controlled Ws2 and Mos2 Sheets by Sulfurization of Thin Metal Films. *Appl. Phys. Lett.* **2014**, *105*, 083112.

(16) Elías, A. L.; Perea-López, N.; Castro-Beltrán, A.; Berkdemir, A.; Lv, R.; Feng, S.; Long, A. D.; Hayashi, T.; Kim, Y. A.; Endo, M. Controlled Synthesis and Transfer of Large-Area Ws2 Sheets: From Single Layer to Few Layers. *ACS Nano* **2013**, *7*, 5235−5242.

(17) Medina, H.; Li, J.-G.; Su, T.-Y.; Lan, Y.-W.; Lee, S.-H.; Chen, C.-W.; Chen, Y.-Z.; Manikandan, A.; Tsai, S.-H.; Navabi, A. Wafer-Scale Growth of Wse2Monolayers toward Phase-Engineered Hybrid Wo X/Wse2 Films with Sub-Ppb No X Gas Sensing by a Low-Temperature Plasma-Assisted Selenization Process. *Chem. Mater.* **2017**, *29*, 1587−1598.

(18) Bäuerle, D. *Laser Processing and Chemistry*; Springer: Berlin, Heidelberg, 2011.

(19) Grigoropoulos, C. P. *Transport in Laser Microfabrication: Fundamentals and Applications*; Cambridge University Press, New York, 2009.

(20) Rho, Y.; Pei, J.; Wang, L.; Su, Z.; Eliceiri, M.; Grigoropoulos, C. P. Site-Selective Atomic Layer Precision Thinning of Mos2 Via Laser-Assisted Anisotropic Chemical Etching. *ACS Appl. Mater. Interfaces* **2019**, *11*, 39385−39393.

(21) Castellanos-Gomez, A.; Barkelid, M.; Goossens, A.; Calado, V. E.; van der Zant, H. S.; Steele, G. A. Laser-Thinning of Mos2: On Demand Generation of a Single-Layer Semiconductor. *Nano Lett.* **2012**, *12*, 3187−3192.

(22) Kim, E.; Ko, C.; Kim, K.; Chen, Y.; Suh, J.; Ryu, S. G.; Wu, K.; Meng, X.; Suslu, A.; Tongay, S. Site Selective Doping of Ultrathin Metal Dichalcogenides by Laser-Assisted Reaction. *Adv. Mater.* **2016**, *28*, 341−346.

(23) Moulder, J. F.; Chastain, J. *Handbook of X-Ray Photoelectron Spectroscopy: A Reference Book of Standard Spectra for Identification and Interpretation of Xps Data*; Physical Electronics Division, Perkin-Elmer Corporation, Eden Prairie, 1992.

(24) Abdallah, W. e. A.; Nelson, A. E. Characterization of Mose2(0001) and Ion-Sputtered Mose2 by Xps. *J. Mater. Sci.* **2005**, *40*, 2679−2681.

(25) Wiegenstein, C. G.; Schulz, K. H. Methanethiol Adsorption on Defective Mos2(0001) Surfaces. *J. Phys. Chem. B* **1999**, *103*, 6913−6918.

(26) Heavens, O. S. *Optical Properties of Thin Solid Films*; Dover: New York, 1991.

(27) Landolt, B.; Börnstein, R. *Thermodynamic Properties of Inorganic Materials*; Springer: Berlin, Heidelberg, 1999.

(28) Shin, B.; Bojarczuk, N. A.; Guha, S. On the Kinetics of MoSe2 Interfacial Layer Formation in Chalcogen-Based Thin Film Solar Cells with a Molybdenum Back Contact. *Appl. Phys. Lett.* **2013**, *102*, 091907.

https://dx.doi.org/10.1021/acs.jpcc.0c04914
J. Phys. Chem. C 2020, 124, 19333−19339